Electronic Supplementary Information

Tunable ratiometric temperature sensors based on a Zn-MOF material incorporating luminescent polyoxometalates and carbon dots.

Cédric Viravaux,[a] Pierre Mialane,[a] Anne Dolbecq,[a] Naseem Ramsahye,[b] Caroline Mellot-Draznieks,[a,c] Hélène Serier-Brault[d,*] and Olivier Oms[a,*]

[a] *Université Paris Saclay, UVSQ, CNRS, Institut Lavoisier de Versailles, 78000 Versailles, France.*

[b] *Institut Charles Gerhardt Montpellier, UMR 5253 CNRS, Université de Montpellier, Place E. Bataillon, 34095 Montpellier Cedex05, France.*

[c] *Laboratoire de Chimie des Processus Biologiques, UMR CNRS 8229, Collège de France, Sorbonne Université, PSL Research University, 11 Place Marcelin Berthelot, 75231 Paris Cedex 05, France.*

[d] *Université de Nantes, CNRS, Institut des Matériaux Jean Rouxel, IMN, F-44000 Nantes, France.*

Table of Content

Optical properties

Experimental section

a) Synthesis

All reagents were purchased and used without further purification except $Na_9[EuW_{10}O_{36}].32H_2O$ (EuW_{10}),[1] green carbon dots (GCDs)[2] and blue carbon dots (BCDs)[3] which have been synthesized according to reported procedures.

Synthesis of $Na_9[EuW_{10}O_{36}].32H_2O$ (EuW_{10}): 2.075 g (6.29 mmol) of $Na_2WO_4.2H_2O$ were dissolved in 5 mL of water and the pH of the solution was adjusted to 7.3 with pure acetic acid. The solution was then heated to 80°C. After 30 minutes, a solution containing 0.275 g (0.616 mmol) of $Eu(NO_3)_3.6H_2O$ in 0.5 mL of water was added dropwise. After a further 30 minutes stirring at 80°C, the solution was cooled to room temperature and allowed to slowly evaporate. After 24 h, 1.21 g of large crystals of $Na_9[EuW_{10}O_{36}].32H_2O$ (0.363 mmol) were recovered, washed with cold water and dried. Yield: 59%.
IR (ATR); ν (cm^{-1}): 3373 (s, br), 1642 (s, br), 1410 (m), 967 (w), 922 (s), 830 (s), 777 (m), 689 (m), 576 (w), 529 (w, br) 406 (m).

Synthesis of green carbon dots (GCDs): 1 g of citric acid (5.20 mmol) and 2 g of urea (33.3 mmol) were dissolved in 10 mL of DMF before being transferred in a Teflon lined stainless steel autoclave and heated at 180°C for 6 h. After the solvothermal synthesis, the mixture was cooled down to room temperature and then filtered. The solvent was evaporated and the residue was purified via silica gel chromatography column, using an increasingly polar gradient of dichloromethane and methanol for the elution. Green carbon dots (GCDs) were isolated after evaporation of the appropriate fractions and then kept at 0°C.

*Synthesis of blue carbon dots (BCDs)***:** 0.210 g of citric acid (1 mmol) and 0.216 g of o-phenylenediamine (2 mmol) were dissolved in 10 mL of ultrapure MilliQ water before being transferred in a Teflon lined stainless steel autoclave and heated up at 160°C for 8 hours. The solution was then centrifugated at 10 000 rpm for 10 min and filtered with a 0.22 µm membrane filter. Finally, the solution was dialyzed for 24 h using a 1KD MWCO membrane. The purified solution has then been freeze-dried overnight and stored at 0°C.

Synthesis of ***EuW_{10}/GCDs@ZIF-8²*** *and* ***EuW_{10}/BCDs@ZIF-8²****:*

Incorporation of CDs and EuW_{10} in ZIF-8² has been performed following a strategy adopted for the incorporation of CDs in ZIF-8².[4] A solution containing 1.115 g of 2-methylimidazole (13.58 mmol) in 5 mL of H_2O was prepared. 1 mg of CTAB (2.74 μmol) was then added under stirring. After one minute, 5 mL of an aqueous solution containing 0.600 g of $Zn(OAc)_2.2H_2O$ (3.27 mmol) was poured into the solution and the resulting mixture stirred for 10 s. Then, an aqueous solution containing the CDs (0.2 mL of a 1 mg/mL GCDs solution or 1 ml of a 1 mg/mL BCDs solution) and 0.5 mL of an aqueous solution containing 20 mg of EuW_{10} were rapidly simultaneously added. The resulting solution was kept under stirring for 10 s and the solution left to stand for 2 h. The mixture was then centrifuged and washed with H_2O. The solid was then redispersed in 15 mL of a methanol solution containing 37 mg of 2-methylimidazole (0.451 mmol) and stirred for 5 min before adding 15 mL of a methanol solution containing 134 mg of $Zn(NO_3)_2.6H_2O$ (0.450 mmol). The mixture was then left to stand for one further hour before being centrifuged. MeOH was then used to wash out the powder until the supernatant no longer showed any luminescence. The **EuW_{10}/GCDs@ZIF-8²** or **EuW_{10}/BCDs@ZIF-8²** were then collected after drying overnight, affording 0.18 g of composite in each case.

Synthesis of ***GCDs@ZIF-8²*** *and* ***BCDs@ZIF-8²***

The synthetic procedure of these two reference materials is similar to that described above except we used 0.5 mL of a 1 mg/mL GCD aqueous solution for **GCDs@ZIF-8²** or 0.2 mL of a 1 mg/mL BCD aqueous solution for **BCDs@ZIF-8²**.

Synthesis of ***EuW_{10}@ZIF-8²***

The synthetic procedure of this reference material is similar to that described above except we used a solution of 20 mg of EuW_{10} dissolved in 0.5 mL of water.

b) Physical Measurements.

Infrared spectra were recorded on a Nicolet 30 ATR 6700 FT spectrometer.

EDX measurements were performed on a JEOL JSM 5800LV apparatus.

Thermogravimetry analyses (TGA) were performed on a Mettler Toledo TGA/DSC 1, STARe System apparatus under oxygen flow (50 mL min^{-1}) at a heating rate of 5°C min^{-1} up to 700°C.

Powder X-ray diffraction (PXRD) data were obtained on a Bruker D5000 diffractometer using Cu radiation (1.54059 Å).

Inductively coupled plasma optical emission spectroscopy (ICP-OES) measurements were carried out using an Agilent 720 Series with axially viewed plasma.

N_2 adsorption/desorption analysis were performed on a Micromeritics Tristar instrument at 77 K (sample activation were carried out at 120°C under vacuum overnight).

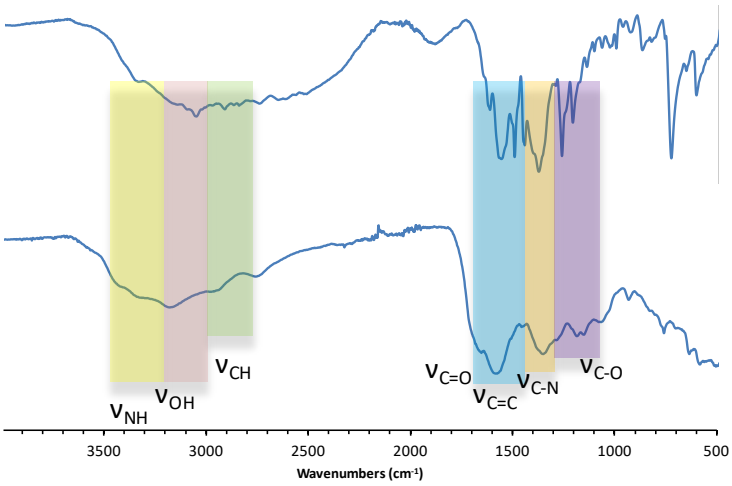

Figure S1: IR spectra of BCDs (top) and GCDs (bottom).

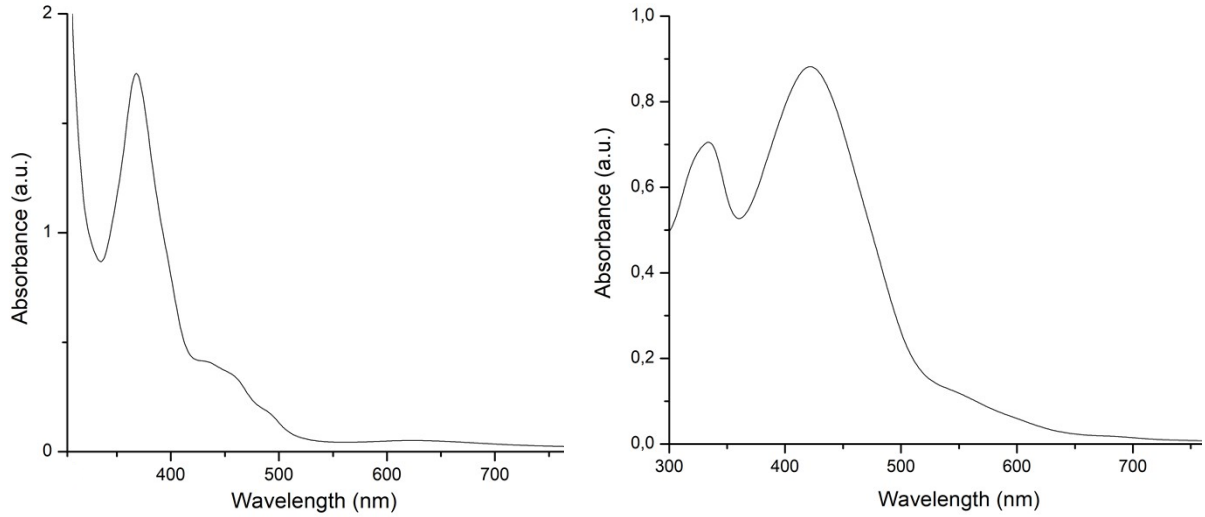

Figure S2: UV-Visible spectra of BCDs (left) and GCDs (right) (solvent: water).

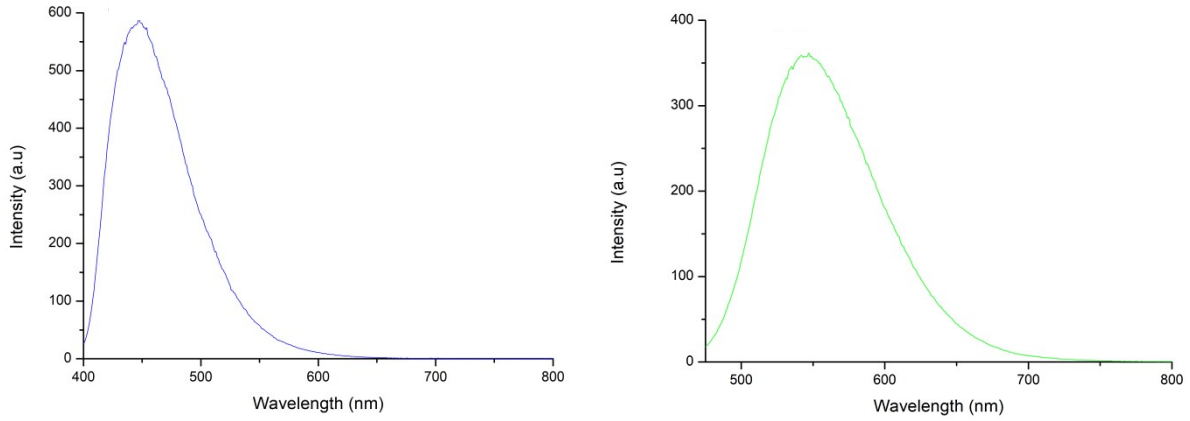

Figure S3: PL spectra of BCDs (left, λ_{exc} = 350 nm) and GCDs (right, λ_{exc} = 450 nm). Solvent: water

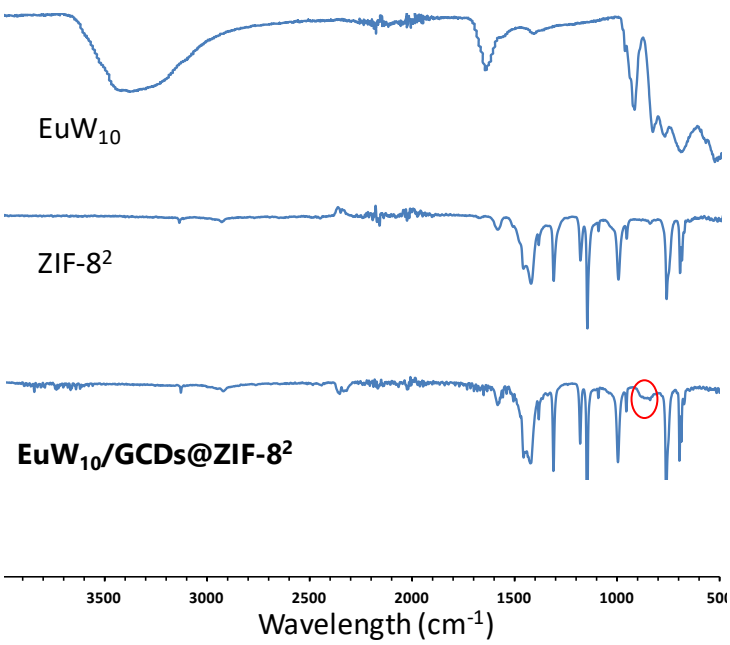

Figure S4: Infrared spectra of EuW_{10}, ZIF-8^2 and **EuW_{10}/GCDs@ZIF-8^2**. For **EuW_{10}/GCDs@ZIF-8^2**, the red circle indicates W-O_b-W vibration bands of the POM entity.

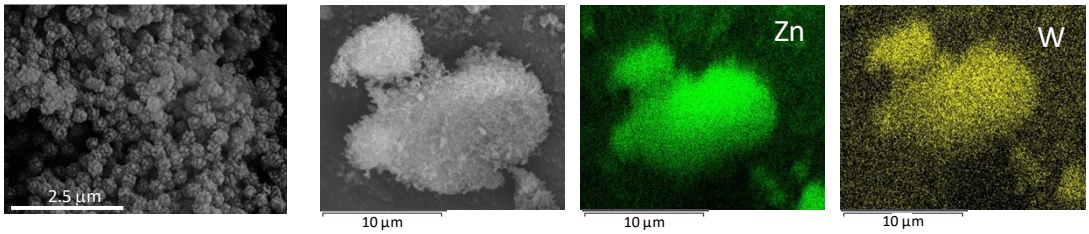

Figure S5: SEM images of **EuW_{10}/GCDs@ZIF-8^2** and EDS mapping for Zn and W.

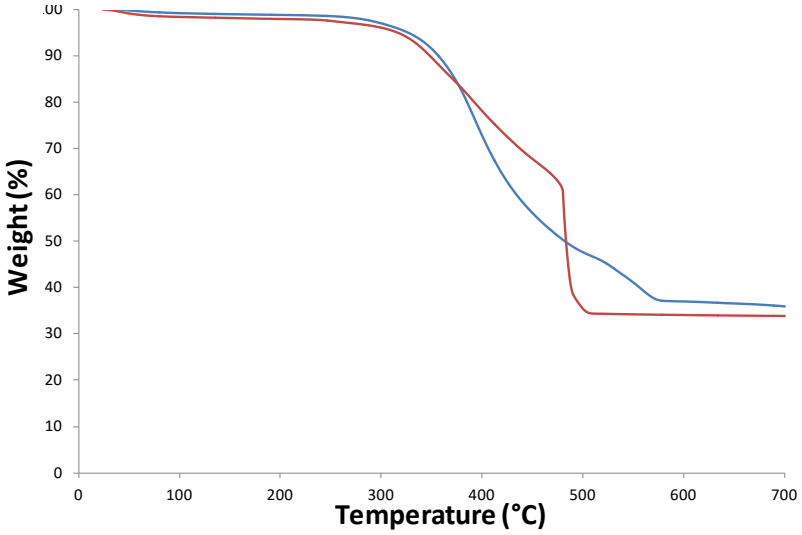

Figure S6: TGA curves of ZIF-8[2] (red line) and **EuW_{10}/GCDs@ZIF-8[2]** (blue line).

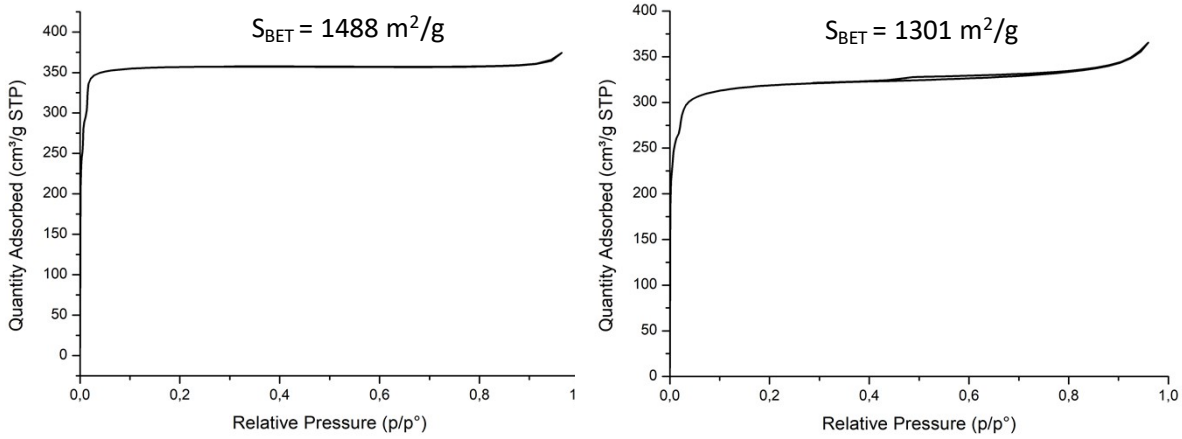

Figure S7: N_2 adsorption-desorption isotherms of ZIF-8[2] (left) and **EuW_{10}/GCDs@ZIF-8[2]** (right).

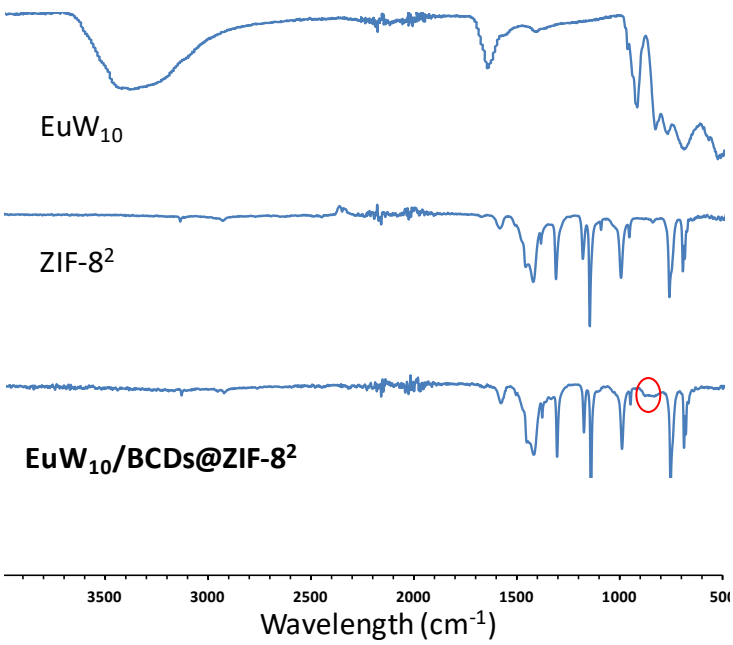

Figure S8: Infrared spectra of EuW_{10}, ZIF-8[2] and **EuW_{10}/BCDs@ZIF-8[2]**. For **EuW_{10}/BCDs@ZIF-8[2]**, the red circle indicates W-O_b-W vibration bands of the POM entity.

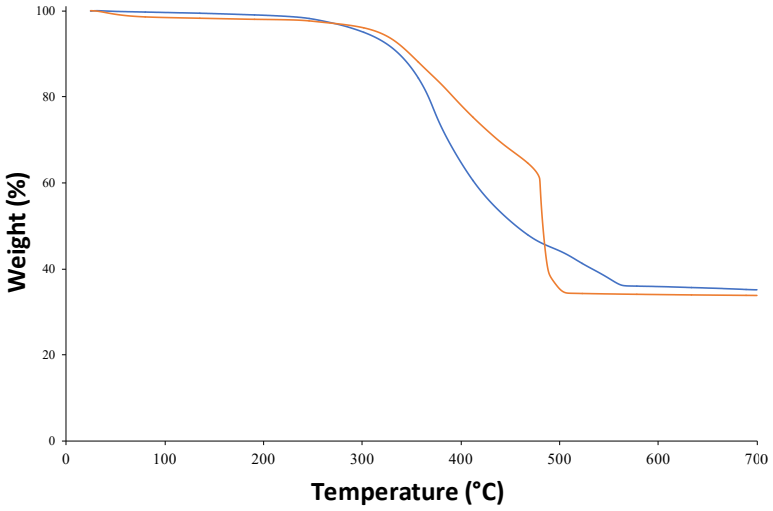

Figure S9: TGA curves of ZIF-8[2] (red line) and **EuW_{10}/BCDs@ZIF-8[2]** (blue line).

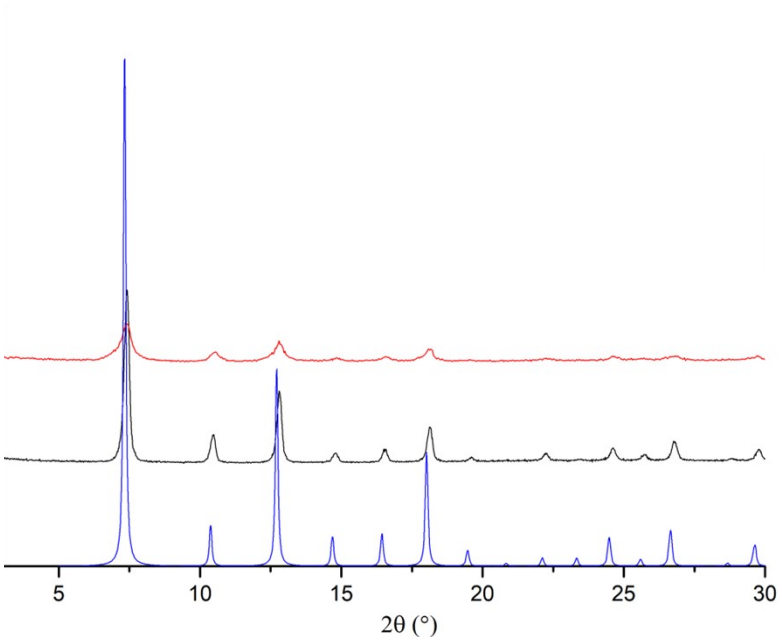

Figure S10: PXRD patterns of ZIF-8[2] (blue: simulated; black: experimental) and **EuW_{10}/BCDs@ZIF-8[2]** (red)

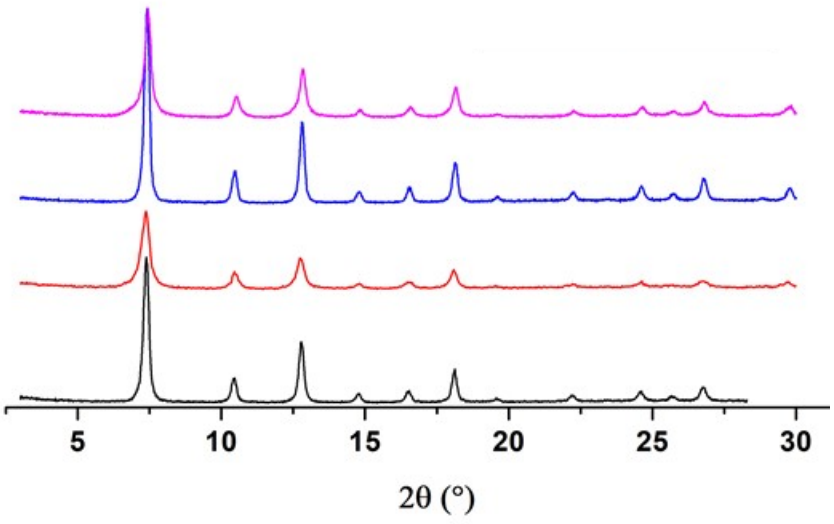

Figure S11: PXRD patterns of ZIF-8[2] (blue), GCDs@ZIF-8[2] (purple), BCDs@ZIF-8[2] (red) and EuW_{10}@ZIF-8[2] (black)

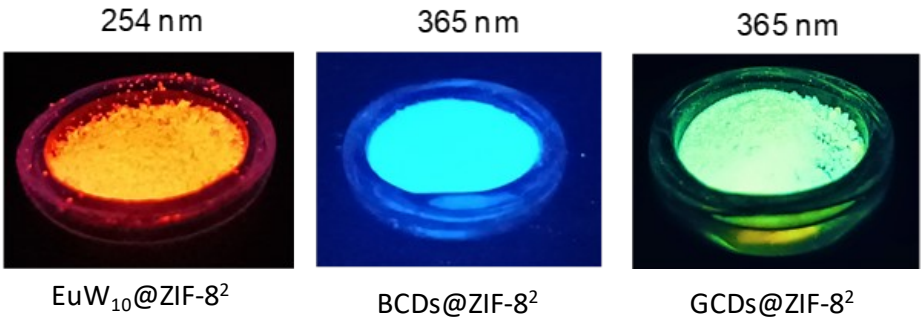

Figure S12: Photographs of EuW_{10}@ZIF-8^2 under 254 nm irradiation (left), BCDs@ZIF-8^2 under 365 nm irradiation (middle) and GCDs@ZIF-8^2 under 365 nm irradiation (right).

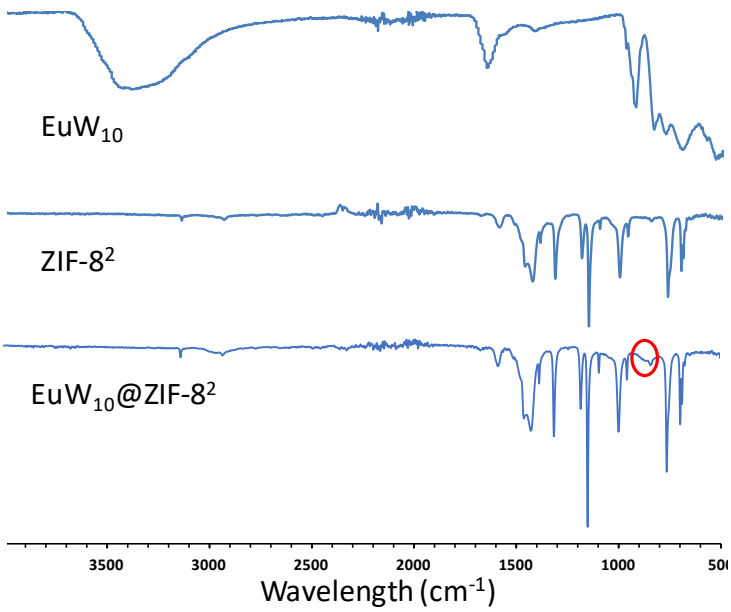

Figure S13: Infrared spectra of EuW_{10}, ZIF-8^2 and EuW_{10}@ZIF-8^2. For EuW_{10}@ZIF-8^2, the red circle indicates W-O_b-W vibration bands of the POM entity.

COMPUTATIONAL SECTION

Creation of the ZIF-8 surface slab

The full procedure for the creation of the ZIF-8 surface is described in detailed in a previously published procedure,[5] and is based on two methodologies originally developed for zeolites[6] and HKUST-1.[7] The main steps of the general method are reminded here, while the reader is directed to reference 5 and its supporting information for full details:

- The bulk unit-cell of ZIF-8 was first geometry-optimized using the Quickstep module of the CP2K software,[8] allowing both the atomic positions of the hybrid framework and the unit-cell parameters to fully relax. The PBE functional[9] was used along with a combined Gaussian basis-set and plane wave pseudopotential strategy as implemented in the code. A triple-ζ Gaussian-type basis-set (TZVP-MOLOPT basis-set provided with the code)[10] was considered for all atoms, except for the metal centers, where double-ζ functions were employed instead (DZVP-MOLOPT).[10] The pseudopotentials used for all of the atoms were those derived by Goedecker, Teter, and Hutter.[11] These calculations included the semi-empirical dispersion corrections as implemented in the DFT-D3 method, derived by Grimme.[12]
- The Bravais-Friedel-Donner-Harker method[13] was used to identify two potential Miller indices that could give plausible surface cuts, the surfaces being cleaved using the Materials Studio Visualiser[14] starting from the above DFT-optimized structure of the ZIF-8. In the present work, we selected the (011) surface to further dock the EuW_{10} POM, as (011) is more stable than the other surface explored, namely the (100) plane.[5] The resulting model possessed the following size, a= 50.98 Å, b = 48.06 Å and c = 146.12 Å, with a slab thickness of 96.8 Å along the z-axis and a 40 Å vacuum gap between the slab and its periodic image in the *z* direction in order to avoid possible

interactions during the subsequent calculation steps.

- Upon cleavage, under-coordinated Zn atoms in the (011) surface result from the elimination of the imidazolate linkers. We further replaced each missing imidazolate linker by a hydroxo and an aqua ligand in order to complete the coordination of the two involved Zn centers, as illustrated in Figure S14. This termination has been previously shown by Sholl *et al.* to be thermodynamically favoured when arising from missing-linker defects.[15] Furthermore, in order to make sure that there was no net dipole in the *z* direction, both surfaces of the slab that are exposed to vacuum were functionalized in a similar fashion with -OH and H_2O in the same positions, i.e. one surface being the mirror image of the other. The manually added -OH and H_2O groups were adjusted through a geometry-optimisation using the *uff* forcefield,[16] keeping the rest of the geometry-optimized ZIF-8 structure fixed.

Defective ZIF-8 structural model

The defective model of ZIF-8 was constructed using the above ZIF-8's structure and removing two additionnal Zn^{2+} centers and their four imidazolate ligands within the bulk of ZIF-8 that are part of the same sodalite-type cage. The coordination of the resulting undercoordinated Zn^{2+} centers was completed by water molecules and -OH groups so as to satisfy the tetrahedral coordination of each Zn^{2+}. The geometry of the added species was further adjusted through a geometry-optimization step using the *uff* forcefield.[16] The resulting structure was used for docking one EuW_{10} POM per cell. In this case, the vacuum gap between the slab and its periodic image was reduced so as to prohibit any insertion of the POM at the (011) surface during the simulated annealing procedure (see below).

Docking of EuW_{10} in ZIF-8 models

For probing the host-guest potential energy surface between the $[EuW_{10}O_{36}]^{9-}$ POM and the ZIF-8 (011) surface and its defective version, we applied a simulated annealing procedure whereby a Monte Carlo Metropolis algorithm is used.[17] Each annealing cycle consisted of 50000 independent Monte Carlo steps per POM, initiating each energy minimization at 1000 K followed by system-cooling to 300 K. Low energy POM adsorption sites were thus identified by searching the configurational space of the $\{[EuW_{10}O_{36}]^{9-}$, ZIF-8$\}$ system as the temperature is slowly decreased. During this conformational search, the $[EuW_{10}O_{36}]^{9-}$ POM was treated as a rigid body and the ZIF-8 as the fixed-atom host. Only the position and orientation of the POM were thus sampled during the simulated annealing procedure while exploring the host. Calculations were performed fixing the loading of POM at 1 per unit-cell. Non-bonded interactions between $[EuW_{10}O_{36}]^{9-}$ and ZIF-8 were described using the universal forcefield *uff*[16] with a real-space cutoff of 43 Å while handling the long-range electrostatic interactions with explicit charges and the Ewald summation technique with a relative precision of 10^{-6}. The atomic charges for ZIF-8 were calculated by the charge-equilibration method,[18] fixing it total charge to +9 to compensate the POM's negative charge. The partial charges of the POM were determined as detailed in the following section.

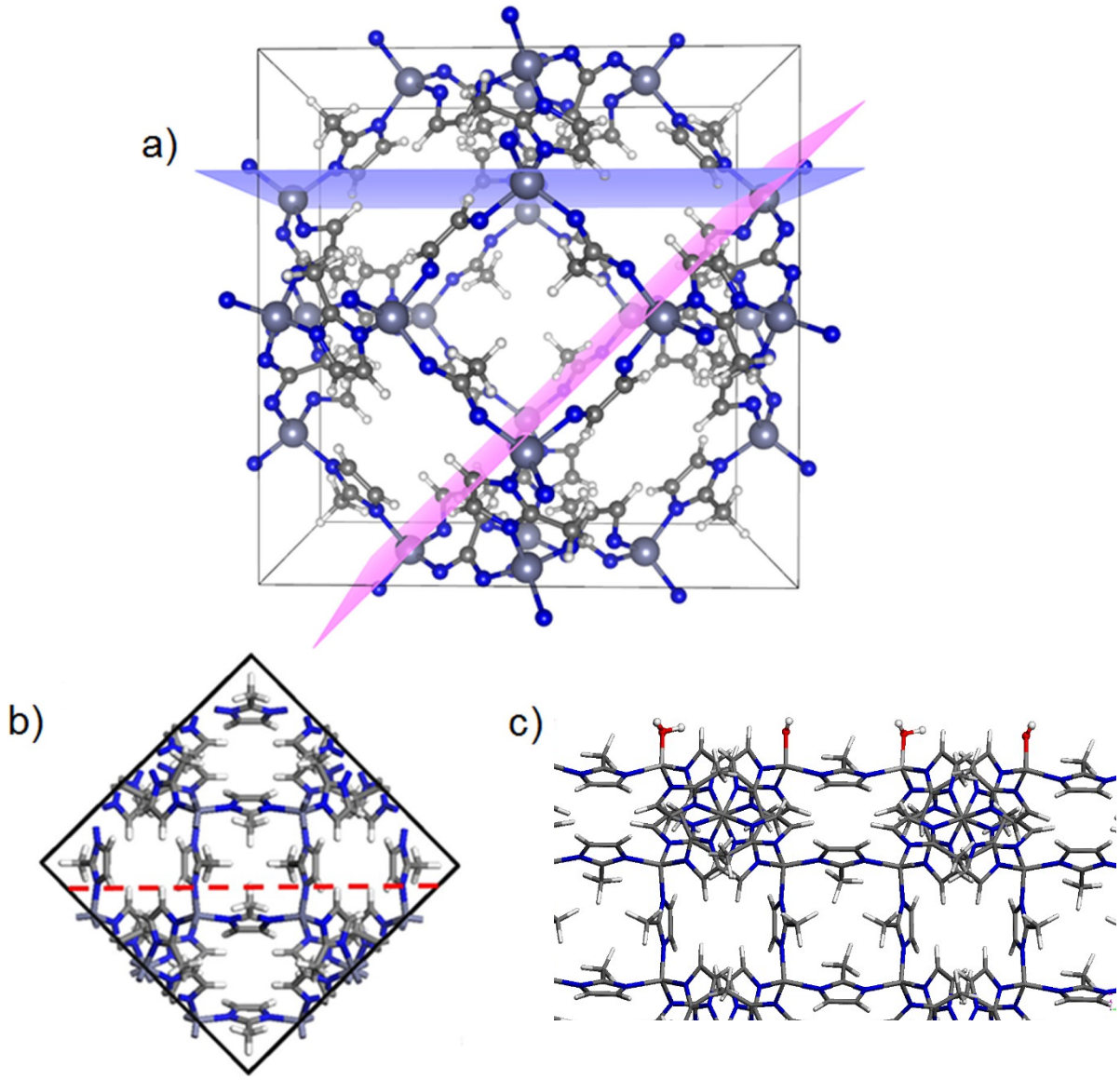

Figure S14: a) The two planes considered for ZIF-8 - the blue one represents the (100) plane, and the pink one the (011) plane. b) The (011) surface cut in the bulk ZIF-8 crystal structure leaves under-coordinated Zn and N atoms. c) Detailed view of the (011) surface showing the H_2O and -OH groups replacing the imidazolate missing linkers.

Partial Charges on the POM

The crystal structure of the analogous POM $Na_9[Dy(W_5O_{18})_2].35H_2O$[19] was used to obtained a DFT geometry-optimized $[EuW_{10}O_{36}]^{9-}$ POM, replacing Dy with Eu in the original CIF file, using the Vienna ab initio simulation package (VASP).[20] The Perdew-Burke-Ernzerhof (PBE) exchange-correlation functional[9] was used along with the semi-empirical vdW method of Grimme DFT-D3.[12] A plane-wave basis set with an energy cutoff

of 400 eV was employed for the geometry optimizations utilizing PAW pseudopotentials on all atoms to describe the electron-ion interactions.[21] Atomic positions were optimized until the forces on all atoms were smaller than 0.02 eV $Å^{-1}$. The Brillouin zone was sampled only at the Γ-point. The atomic partial charges on this DFT-optimised POM model were then extracted using the DMol^3 code,[22] and the PBE GGA functional.[9] The DNP numerical basis set[23] was applied to all of the atoms, and the effect of solvation was considered using the COSMO model,[24] setting a dielectric constant of 78.4, to simulate the presence of water. A total charge of -9 was applied to the model, considering a septet configuration for the spin multiplicity. The electrostatic potential (ESP) partial atomic charges were subsequently extracted, and are shown in Figure S15.

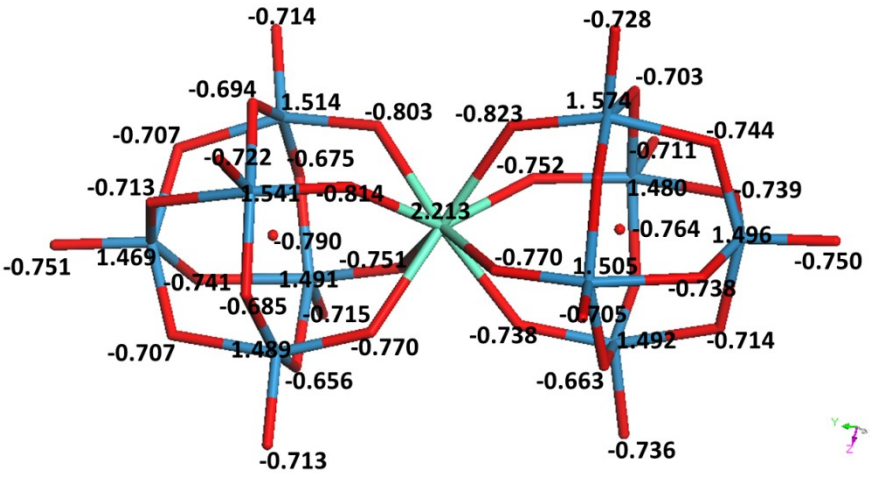

Figure S15: The ESP partial charges calculated for the $[EuW_{10}O_{36}]^{9-}$ POM atoms. The blue atoms are W, red are O and cyan represents Eu.

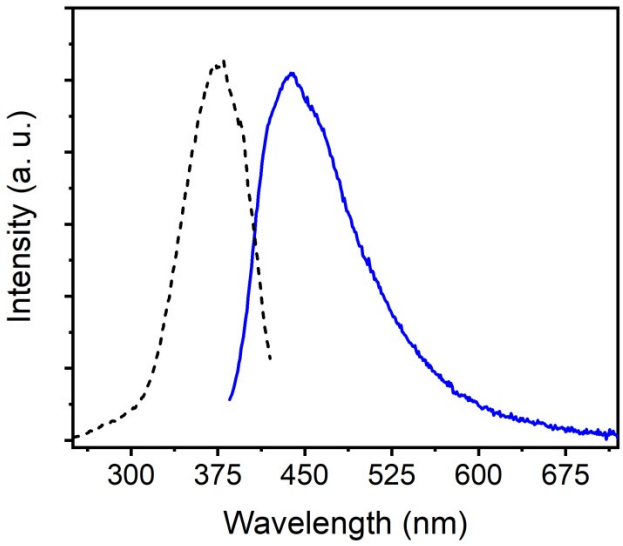

Figure S16: Room-temperature excitation spectrum (black dotted line, λ_{em} = 438 nm) and emission spectrum (blue line, λ_{exc} = 375 nm) of ZIF-8[2] MOF.

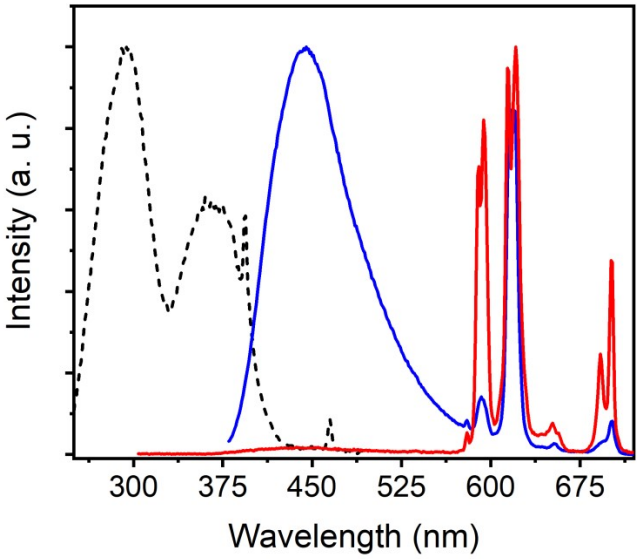

Figure S17: Room-temperature excitation spectrum (black dotted line, λ_{em} = 612 nm) and emission spectra monitored at λ_{exc} = 375 nm (blue line) and at λ_{exc} = 294 nm (red line) of EuW_{10}@ZIF-8[2] MOF.

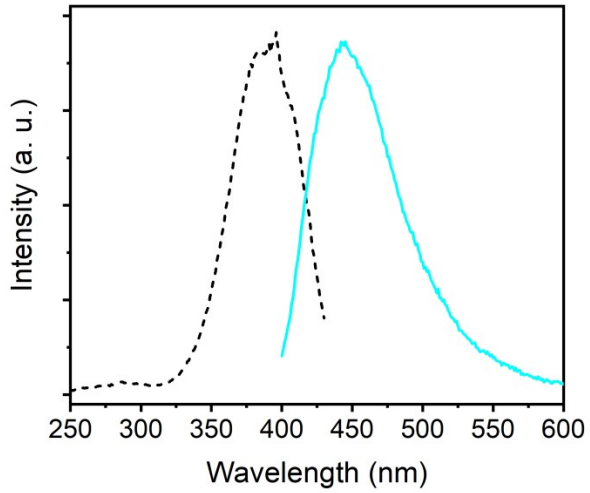

Figure S18: Room-temperature excitation spectrum (black dotted line, λ_{em} = 443 nm) and emission spectrum (cyan line, λ_{exc} = 370 nm) of BCDs@ZIF-8[2] MOF.

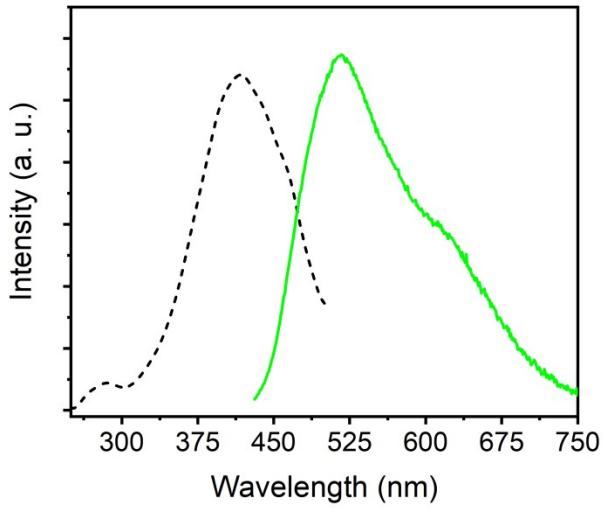

Figure S19: Room-temperature excitation spectrum (black dotted line, λ_{em} = 516 nm) and emission spectrum (green line, λ_{exc} = 418 nm) of GCDs@ZIF-8[2] MOF.

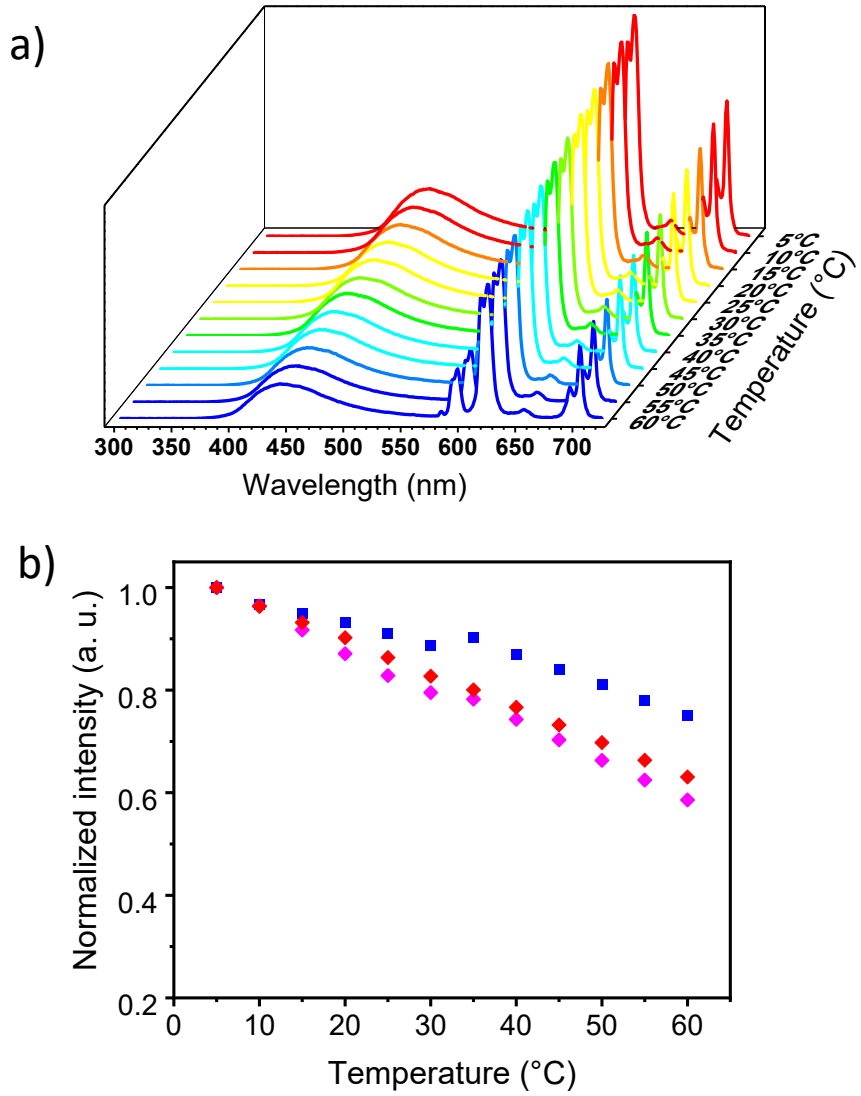

Figure S20: a) Emission spectra of **EuW_{10}/BCDs@ZIF-8**[2] in the 5-60°C range with the excitation fixed at 294 nm; b) thermal evolution of I_{BCDs} (blue) and I_{Eu} at 594 nm ($^5D_0$ ➲ $^7F_1$ transition in pink) and at 612 nm ($^5D_0$ ➲ $^7F_2$ transition, in red).

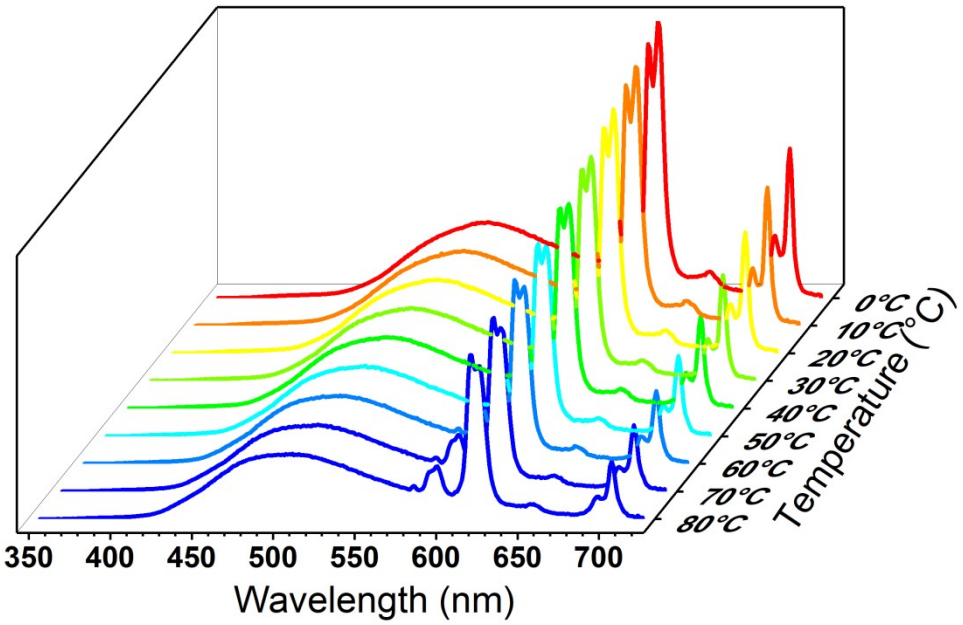

Figure S21: Emission spectra of **EuW_{10}/GCDs@ZIF-8**[2] in the 5-80°C range with the excitation fixed at 294 nm.

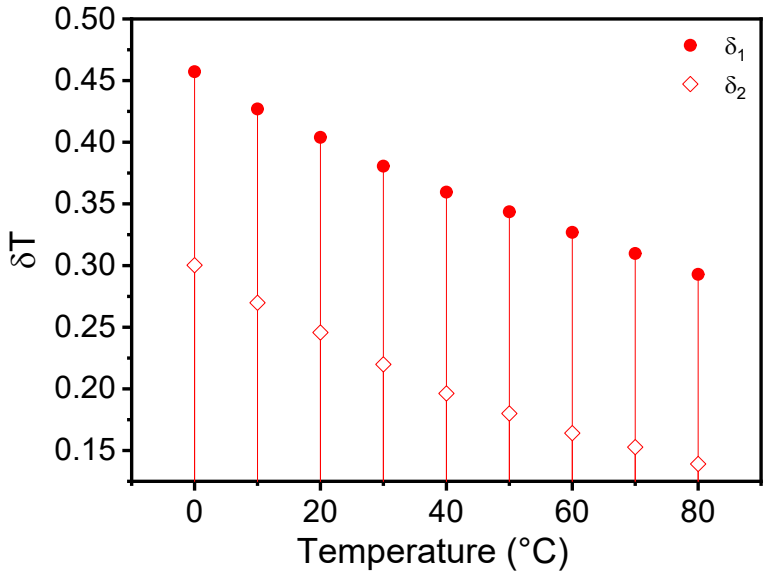

Figure S22. Minimal temperature uncertainty ($\delta T = {}^{1}/_{S_r} \times \delta\Delta/\Delta$), in the 0-80°C range ($\delta\Delta/\Delta$ was estimated as 0.2% for a photomultiplier) for the compound **EuW_{10}/GCDs@ZIF-8**[2] when using the thermometric parameter $\Delta_1 = I_{Eu1}/I_{GCDs}$ and $\Delta_2 = I_{Eu2}/I_{GCDs}$, respectively.

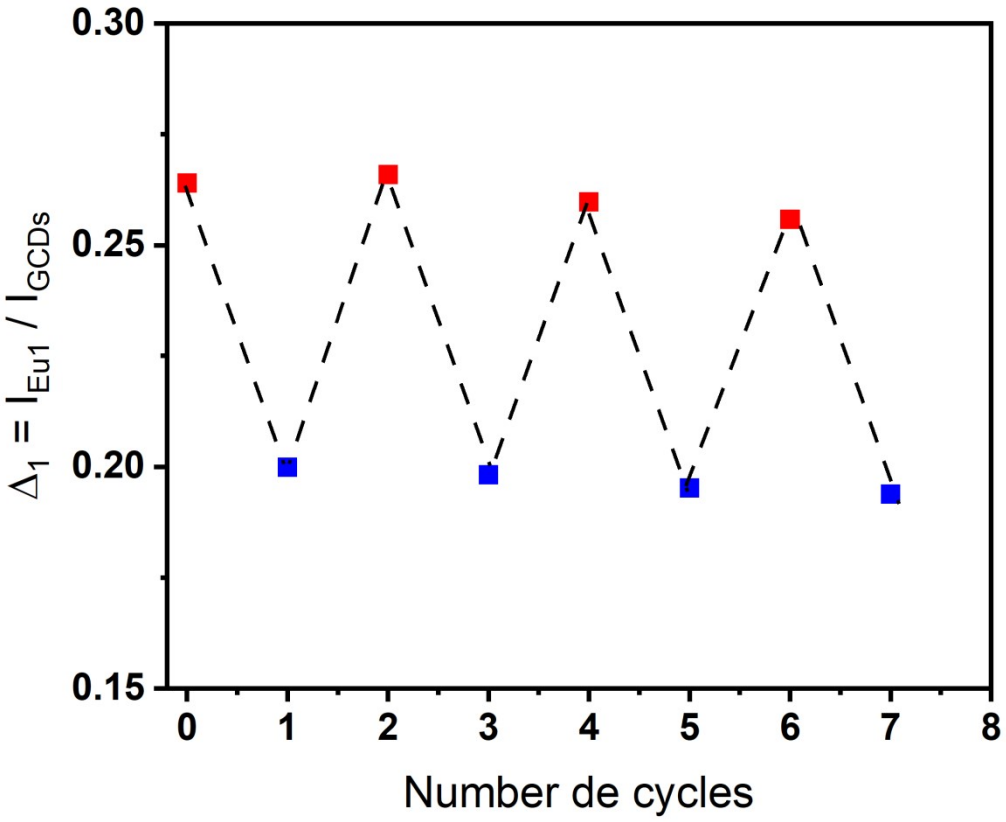

Figure S23: Temperature cycling between 0 °C (blue dots) and 80°C (red dots) revealing a repeatability > 97% for **EuW_{10}/GCDs@ZIF-8**[2].

References

[1] M. Sugeta and T. Yamase, *Bull. Chem. Soc. Jpn.*, 1993, **66**, 444–449.

[2] T. Hu, Z. Wen, C. Wang, T. Thomas, C. Wang, Q. Song and M. Yang, *Nanoscale Adv*., 2019, **1**, 1413-1420.

[3] A. Tan, G. Yang and X. Wan, *Spectrochim. Acta A Mol. Biomol. Spectrosc.*, 2021, **253**, 119583.

[4] Y. Ding, Y. Lu, K. Yu, S. Wang, D. Zhao and B. Chen, *Adv. Optical Mater*., 2021, **9**, 2100945.

[5] R. Semino, N.A. Ramsahye, A. Ghoufi and G. Maurin, *ACS Appl. Mater. Interfaces*, 2016, **8**, 809−819.

[6] B. Slater, J. O. Titiloye, F. M. Higgins and S. C. Parker, *Curr. Opin. Solid State Mater. Sci.*, 2001, **5**, 417−424.

[7] S. Amirjalayer, M. Tafipolsky and R. Schmid, *J. Phys. Chem. Lett.*, 2014, **5** (18), 3206−3210.

[8] J. Hutter, M. Iannuzzi, F. Schiffmann and J. VandeVondele, CP2K: Atomistic Simulations of Condensed Matter Systems. *Wiley Interdiscip. Rev.: Comput. Mol. Sci.* 2014, **4** (1), 15−25.

[9] J.P. Perdew, K. Burke and M. Ernzerhof, *Phys. Rev. Lett.* 1996, **77**, 3865−3868.

[10] J. Van de Vondele and J. Hutter, *J. Chem. Phys.*, 2007, **127** (11), 114105.

[11] S. Goedecker, M. Teter and J. Hutter, J. *Phys. Rev. B: Condens. Matter Mater. Phys.*, 1996, **54**, 1703−1710.

[12] (a) S. Grimme, *J. Comput. Chem.*, 2006, **27** (15), 1787−1799. (b) S. Grimme, J. Antony, S. Ehrlich and H. Krieg, *J. Chem. Phys.*, 2010, **132**, 154104.

[13] (a) J. D. Donnay and G. Harker, *Am. Mineral.* 1937, **22**, 446−467. (b) G. Friedel, *Bull. Soc. Fr. Mineral.*, 1907, **30**, 326−455. (c) A. Bravais, *Etudes Cristallographiques*; Gauthier-Villars: Paris, 1866.

[14] *Materials Sudio,* Accelrys Suite of Software Inc., 2001.

[15] (a) C. Zhang, C. Han, D. S. Sholl and J. R. Schmidt, *J. Phys. Chem. Lett*., 2016, **7** (3), 459–

464. (b) C. Han, R. J. Verploegh and D. S. Sholl, *J. Phys. Chem. Lett.*, 2018, **9**, 4037-4044.

[16] (a) A. K. Rappé, C. J. Casewit, K. S. Colwell, W. A. Goddard and, W. M. Skiff, *J. Am. Chem. Soc.* 1992, **114**, 10024; (b) A. K. Rappé, K. S. Colwell and, C. J. Casewit, *Inorg. Chem.*, 1993, **32**, 3438.

[17] N. Metropolis, A. Rosenbluth, M. Rosenbluth, A. Teller and E. Teller, *J. Chem. Phys.*, 1953, **21**, 1087.

[18] A. K. Rappé and, W. A. Goddard III. *J. Phys. Chem.*, 1995, **95**, 3358.

[19] K. Sawada and T. Yamase, *Acta Cryst. C.*, 2002, **C58**, i149-i151.

[20] G. Kresse and Furthmüller, *J. Phys. Rev. B*, 1996, **54**, 11169–11186.

[21] (a) P. E. Blöchl, *Phys. Rev. B*, 1994, **50**, 17953-17979. (b) G. Kresse and D. Joubert, *Phys. Rev. B* 1999, **59**, 1758-1775.

[22] B. Delley, *J. Chem. Phys.,* 2000, **113**, 7756. *Materials Sudio,* Accelrys Software Inc., 2001.

[23] B. Delley, *J. Chem. Phys.*, 1990, **92**, 508−517.

[24] A. Klamt and G. Schuurmann, *J. Chem. Soc., Perkin Trans. 2*, 1993, 799-805.